F.E. simulation of biomechanical problems with a hyperelastic anisotropic four-fibre polyconvex law

Wael Alliliche, Christine Renaud, Jean Michel Cros, Zhi Qiang Feng

▶ **To cite this version:**

Wael Alliliche, Christine Renaud, Jean Michel Cros, Zhi Qiang Feng. F.E. simulation of biomechanical problems with a hyperelastic anisotropic four-fibre polyconvex law. 25e Congrès Français de Mécanique, Nantes, 29 août-2 septembre 2022, Aug 2022, Nantes, France. hal-04280017

HAL Id: hal-04280017
https://hal.science/hal-04280017

Submitted on 10 Nov 2023

HAL is a multi-disciplinary open access archive for the deposit and dissemination of scientific research documents, whether they are published or not. The documents may come from teaching and research institutions in France or abroad, or from public or private research centers.

L'archive ouverte pluridisciplinaire **HAL**, est destinée au dépôt et à la diffusion de documents scientifiques de niveau recherche, publiés ou non, émanant des établissements d'enseignement et de recherche français ou étrangers, des laboratoires publics ou privés.

F.E. simulation of biomechanical problems with a hyperelastic anisotropic four-fibre polyconvex law

W. Alliliche[a], C. Renaud[b], J.-M. Cros[c], Z.-Q. Feng[d],

a. Université Paris-Saclay, Univ Evry, LMEE, Evry, 91020, France, wael.alliliche@univ-evry.fr
b. Université Paris-Saclay, Univ Evry, LMEE, Evry, 91020, France, christine.renaud@univ-evry.fr
c. Université Paris-Saclay, Univ Evry, LMEE, Evry, 91020, France, jeanmichel.cros@univ-evry.fr
d. Université Paris-Saclay, Univ Evry, LMEE, Evry, 91020, France, zhiqiang.feng@univ-evry.fr

Abstract :

The living tissues behave in a hyperelastic anisotropic manner. This study aims to evaluate a recent hyperelastic anisotropic four-fibre polyconvex constitutive law to model soft tissues, such as the skin. This model is implemented in an in-house finite element code to benefit from tools such as the bipotential contact method. A biaxial tensile test is simulated and the results are compared with a semi-analytic solution and experimental data. A simulation of an indentation test using the bipotential contact law is also performed.

Keywords : Biomechanics, soft tissues, anisotropic hyperelastic materials, convexity.

1 Introduction

Most organs that make up the human body are soft tissues, such as the arteries, heart, intestines and skin. The ability to predict human skin behaviour and evaluate changes in the mechanical properties of the tissue would inform engineering design. It would prove valuable in various disciplines: medical research, prosthesis design or 3D modelling for movies and video games. Soft tissues usually contain a basic material called matrix, in which collagen and elastin fibres are distributed. These fibres give the most important characteristics of the tissue. Collagen fibres provide the ability [1] to resist traction. Elastin helps to maintain organ elasticity. Collagen and elastin are perpendicular to each other. A soft tissue behaves as a hyperelastic material. It is almost incompressible because it is mainly made of water [2]. Moreover, it is anisotropic due to the collagen and elastin fibres. Many constitutive laws are used to model soft tissues in the literature. Some represent isotropic behaviour, such as neo-Hookean [3], Mooney-Rivlin [4], 8-chain [5], Yeoh [6], and Gent [7] models. The main difference between them is the trend of the stress-strain curve. Other laws describe both the isotropic and anisotropic behaviours, for example, the HGO [8], and the polyconvex [9] models. In this paper, the latter four-fibre anisotropic polyconvex law is described as well as its implementation. This law has two main properties, the convexity of its strain energy function ensures the existence and uniqueness of the solution, and the invariants used have a mechanical meaning. The procedure for identifying the law parameters from experimental data is described. Simulations of tensile and indentation (3D) tests on soft tissue are performed. The results are compared with those obtained by other laws with a discussion on the simulation times.

2 Polyconvex constitutive law analysis

In this section, the main characteristics of this recent [9] hyperelastic anisotropic behaviour law is given. Previously classical notations of continuum mechanics are reminded. Some standard notations for tensor and vector calculus are recalled: The standard Euclidean inner product is defined by $\langle .,. \rangle$, the product between two vectors and between two tensors are determined by $(. \otimes .)$, the trace operator will be denoted by Tr and the determinant by det.

The transformation tensor $\mathbf{F}$, the right Cauchy-Green strain tensor $\mathbf{C}$, the Green-Lagrange strain tensor $\mathbf{E}$ and the Cauchy stress tensor respectively defined:

$$\mathbf{F} = \mathbf{I} + \frac{\partial \mathbf{u}}{\partial \mathbf{X}}, \quad \mathbf{C} = \mathbf{F}^T \mathbf{F}, \quad \mathbf{E} = \tfrac{1}{2}(\mathbf{C} - \mathbf{I}), \quad \boldsymbol{\sigma} = J^{-1}\mathbf{F}\mathbf{S}\mathbf{F}^T, \tag{1}$$

where $\mathbf{u}$ is the displacement vector in the Lagrangian description and $\mathbf{X}$ is the Lagrangian coordinates representing the initial position, $\mathbf{I}$ stands for the unity tensor, $J = det(\mathbf{F})$.

A material with four fibre directions a, b, c and d (Fig. 6) is considered and $\mathbf{e_1}$, $\mathbf{e_2}$ and $\mathbf{e_3}$ constitute an orthonormal basis. In the plane $\{\mathbf{e_1}, \mathbf{e_2}\}$, fibres a and b are symmetrically distributed around $\mathbf{e_1}$, the fibre directions c and d are parallel to $\mathbf{e_1}$ and $\mathbf{e_1}$ respectively. Cai et al. [9] demonstrated, taken account orthotropic symmetry with respect to three orthogonal planes normal to $\mathbf{e_1}, \mathbf{e_2}, \mathbf{e_3}$, that the seven following polyconvex invariants L_i form an integrity basis which contain all the information relative to the geometrical orientation of the fibres:

$$L_1 = Tr(\mathbf{C}\,\mathbf{e_1} \otimes \mathbf{e_1}),\ L_2 = Tr(\mathbf{C}\,\mathbf{e_2} \otimes \mathbf{e_2}),\ L_3 = Tr(\mathbf{C}\,\mathbf{e_3} \otimes \mathbf{e_3}), \tag{2}$$

$$L_4 = (L_1 + L_2)^2 + 4\langle \mathbf{C}\,\mathbf{e_1}, \mathbf{e_2}\rangle^2, \tag{3}$$

$$L_5 = (L_1 + L_3)^2 + 4\langle \mathbf{C}\,\mathbf{e_1}, \mathbf{e_3}\rangle^2,\ L_6 = (L_2 + L_3)^2 + 4\langle \mathbf{C}\,\mathbf{e_2}, \mathbf{e_3}\rangle^2, \tag{4}$$

$$\begin{aligned} L_7 = {} & \langle \mathbf{C}\,\mathbf{e_1}, \mathbf{e_2}\rangle\langle \mathbf{C}\,\mathbf{e_1}, \mathbf{e_3}\rangle\langle \mathbf{C}\,\mathbf{e_2}, \mathbf{e_3}\rangle \\ & + \tfrac{1}{2}\left(L_1\,L_2\,L_3 - L_1\langle \mathbf{C}\,\mathbf{e_2}, \mathbf{e_3}\rangle^2 - L_2\langle \mathbf{C}\,\mathbf{e_1}, \mathbf{e_3}\rangle^2 - L_3\langle \mathbf{C}\,\mathbf{e_1}, \mathbf{e_2}\rangle^2\right) \end{aligned} \tag{5}$$

In addition to mathematical properties (polyconvexity), these invariants have a mechanical meaning. The first tree are related to the elongations according to $\mathbf{e_1}$, $\mathbf{e_2}$ and $\mathbf{e_3}$ and the next three to the shear according to the directions $\{\mathbf{e_1}, \mathbf{e_2}\}$, $\{\mathbf{e_1}, \mathbf{e_3}\}$ and $\{\mathbf{e_2}, \mathbf{e_3}\}$. The last one is directly linked to the deformed volume. Moreover, to avoid a redundancy with the incompressibility condition which will be expressed explicitly, the invariant L_7 will not be retained in the following.

The strain energy function or polyconvex deformation energy density function, proposed by Cai et al. [9, 10], is a quadratic polynomial form:

$$\begin{aligned} W = {} & a_1\,(L_1 - 1) + a_2\,(L_2 - 1) + a_3\,(L_3 - 1) + a_4\,(L_4 - 4) + a_5\,(L_5 - 4) \\ & + a_6\,(L_6 - 4) + a_7\,(L_1 - 1)^2 + a_8\,(L_2 - 1)^2 + a_9\,(L_3 - 1)^2, \end{aligned} \tag{6}$$

where the coefficients a_i represent the nine material parameters. Using stressless state in the reference configuration, only 7 parameters are independent. The polynomial form has several advantages [9], notably it facilitates the identification of the material parameters.

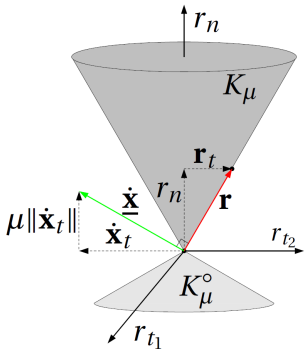

Figure 1: Coulomb's cone representation

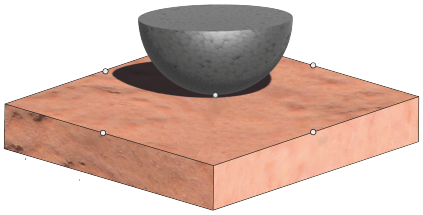

Figure 2: Indentation model

3 Bipotential contact law

The bipotential method [11] is used for the numerical modelling of contact problems, especially the indentation test in this article. The bipotential method can be summarised by writing the Signorini conditions and the Coulomb friction laws in a compact form. This method is more efficient because it considers the coupling of the normal force and the tangential force in the same formulation of the contact laws and does not use the penalty term that induces interpenetration. The bipotential method translates the complete law of contact with friction into a complementarity constraint. Figure 1 represents the contact reaction $\mathbf{r}$ and its components $(\mathbf{r}_t, r_n)$ as well as the tangential relative velocity $\dot{\underline{\mathbf{x}}}$. The complementary relation is written as follows :

$$\dot{\underline{\mathbf{x}}} = \dot{\mathbf{x}}_t + (\dot{x}_n + \mu\|\dot{\mathbf{x}}_t\|)\,\mathbf{n}. \tag{7}$$

K_μ represents the interior and the edge of the Coulomb cone (Fig.1). So, the function b_c is introduced $b_c(-\dot{\mathbf{x}}, \mathbf{r}) = \mu\,\|-\dot{\mathbf{x}}_t\|\,r_n$ if $\dot{x}_n \geq 0$ and $\mathbf{r} \in K_\mu$, and equal to $+\infty$ otherwise. b_c is a bi-potential function which can be interpreted as the dissipated power.

The minus sign preceding the relative tangential velocity emphasizes its opposite direction to the frictional force. According to the Implicit Standard Material theory proposed by De Saxcé and Feng, the complete law of contact with friction is in the form of a variational in-equation. The augmented Lagrangian method was using to solve the following implicit problem :

$$\begin{cases} \text{find} \quad \mathbf{r} \in K_\mu \quad \text{such as} \\ \forall \mathbf{r}' \in K_\mu; \quad \Big(\mathbf{r} - \Big(\mathbf{r} - \varrho\big(\dot{\mathbf{x}}_t + (\dot{x}_n + \mu\|-\dot{\mathbf{x}}_t\|)\,\mathbf{n}\big)\Big)\Big)\cdot(\mathbf{r}' - \mathbf{r}) \geq 0. \end{cases} \tag{8}$$

with $\varrho > 0$, a parameter whose value ensures a good convergence.

However, we must find $\mathbf{r} \in K_\mu$ in such a way

$$\forall \mathbf{r}' \in K_\mu, \quad (\mathbf{r} - \boldsymbol{\tau}) \cdot (\mathbf{r} - \mathbf{r}') \geq 0, \tag{9}$$

where $\boldsymbol{\tau}$, the contact reaction is given:

$$\boldsymbol{\tau} = \mathbf{r} - \varrho\big(\dot{\mathbf{x}}_t + (\dot{x}_n + \mu\|-\dot{\mathbf{x}}_t\|)\,\mathbf{n}\big). \tag{10}$$

$\mathbf{r}$ is the projection of $\boldsymbol{\tau}$ in the Coulomb cone.

The projection ($\mathbf{r} = \mathrm{Proj}_{K_\mu}(\boldsymbol{\tau})$) can be determined analytically. The expressions of the projection can only correspond to three possible contact statuses: contact with adhesion, contact with sliding and with no contact.

$$\begin{array}{lll} \text{if} & \mu \, \|\boldsymbol{\tau_t}^{k+1}\| < -\tau_n^{k+1} \;\; \text{so} \;\; \mathrm{Proj}_{K_\mu}(\boldsymbol{\tau}^{k+1}) = 0 & \text{no contact} \\ \text{else if} & \|\boldsymbol{\tau_t}^{k+1}\| < \mu \, \tau_n^{k+1} \quad \text{so} \;\; \mathrm{Proj}_{K_\mu}(\boldsymbol{\tau}^{k+1}) = \boldsymbol{\tau}^{k+1} & \text{adhesion} \\ \text{else} & \mathrm{Proj}_{K_\mu}(\boldsymbol{\tau}^{k+1}) = \boldsymbol{\tau}^{k+1} - \dfrac{(\|\boldsymbol{\tau}_t^{k+1}\| - \mu \, \tau_n^{k+1})}{(1+\mu^2)} \Big(\dfrac{\boldsymbol{\tau}_t^{k+1}}{\|\boldsymbol{\tau}_t^{k+1}\|} + \mu \, \mathbf{n} \Big) & \text{sliding} \end{array} \tag{11}$$

4 Finite Element Implementation

The polyconvex constitutive law is implemented in our in-house [12] finite element software FER. The nonlinear geometric analysis is described using the total Lagrangian formulation, where the tangent stiffness matrix is built with respect to the initial configuration.

The Green–Lagrangian strain $\mathbf{E}$ can be written [13] with linear $\mathbf{B}_{\mathrm{L}}$ and nonlinear terms $\mathbf{B}_{\mathrm{NL}}$ depending on nodal displacements, either in incremental form:

$$\delta \mathbf{E} = (\mathbf{B}_{\mathrm{L}} + \mathbf{B}_{\mathrm{NL}}(\mathbf{u})) \, \delta \mathbf{u} \tag{12}$$

Based on the principle of virtual displacement, the virtual work δw is:

$$\delta w = \int_{V_0} \delta \mathbf{E}^T \, \mathbf{S} \, dV_0 - \delta \mathbf{u}^T \, \mathbf{F}_{\mathrm{ext}} - \delta \mathbf{u}^T \, \mathbf{R} = 0 \tag{13}$$

where V_0 is the initial volume, $\mathbf{F}_{\mathrm{ext}}$ the vector of external loads, $\mathbf{R}$ the contact reaction vector (section 3). The vector $\mathbf{R}$ in the global reference frame was building from $\mathbf{r}$ (Eq. 11).

Since $\delta \mathbf{u}$ is arbitrary, the non-linear govern equations can be given as:

$$\mathbf{F}_{\mathrm{int}} - \mathbf{F}_{\mathrm{ext}} - \mathbf{R} = 0, \tag{14}$$

where $\mathbf{F}_{\mathrm{int}}$ is the vector of internal forces, which can be defined:

$$\mathbf{F}_{\mathrm{int}} = \int_{V_0} (\mathbf{B}_L + \mathbf{B}_{NL}(\mathbf{u}))^T \, \mathbf{S} \, dV_0 \tag{15}$$

The second Piola-Kirchhoff stress tensor $\mathbf{S}$ is calculated by deriving the strain energy function (6) with respect to the tensor $\mathbf{C}$:

$$\mathbf{S} = 2 \, \frac{\partial W}{\partial \mathbf{C}} - p \, \mathbf{C}^{-1} = 2 \sum_{i=1}^{6} \frac{\partial W}{\partial L_i} \, \frac{\partial L_i}{\partial \mathbf{C}} - p \, \mathbf{C}^{-1}. \tag{16}$$

where p is the external pressure to take into account the incompressibility condition.

Eq. (14) is solved [13] with the Newton-Raphson method.

5 Material parameters identification

The identification of the material parameters is carried out using experimental data. Data [14] from a biaxial quasi-static tensile test on a superficial femoral artery was used.

Cai et al. [9, 10] have given the semi-analytical solution of this biaxial tensile test. With symmetries, one eighth (Figure 3) of the soft tissue sample is studied. Stretches λ_{11} and λ_{22} are imposed respectively along the $\vec{e_1}$ and $\vec{e_2}$ axes. The two non-zero components of the Cauchy stress tensor are written:

$$\begin{aligned}\sigma_{11} &= 2\,a_3(\lambda_{11}^2 - \lambda_{11}^{-2}\lambda_{22}^{-2}) + 4\,a_4(\lambda_{11}^4 + \lambda_{11}^2\lambda_{22}^2 - 2\,\lambda_{11}^2)\\ &\quad + 4\,a_5(\lambda_{11}^4 - \lambda_{11}^{-4}\lambda_{22}^{-4}) + 4\,a_6(2\lambda_{11}^2 - \lambda_{11}^{-2} - \lambda_{11}^{-4}\lambda_{22}^{-4})\\ &\quad + 4\,a_7(\lambda_{11}^4 - \lambda_{11}^2) + 4\,a_9(\lambda_{11}^{-2}\lambda_{22}^{-2} - \lambda_{11}^{-4}\lambda_{22}^{-4}),\end{aligned} \tag{17}$$

$$\begin{aligned}\sigma_{22} &= 2\,a_3(\lambda_{22}^2 - \lambda_{11}^{-2}\lambda_{22}^{-2}) + 4\,a_4(\lambda_{22}^4 + \lambda_{11}^2\lambda_{22}^2 - 2\,\lambda_{22}^2)\\ &\quad + 4\,a_5(2\lambda_{22}^2 - \lambda_{22}^{-2} - \lambda_{11}^{-4}\lambda_{22}^{-4}) + 4\,a_6(\lambda_{22}^4 - \lambda_{11}^{-4}\lambda_{22}^{-4})\\ &\quad + 4\,a_8(\lambda_{22}^4 - \lambda_{22}^2) + 4\,a_9(\lambda_{11}^{-2}\lambda_{22}^{-2} - \lambda_{11}^{-4}\lambda_{22}^{-4}),\end{aligned} \tag{18}$$

where λ_{11}, λ_{22} represent the principal stretches.

Minimisation of the error between these data has been performed with optimisation constraints using MATLAB *fmincon* function [15] . To ensure the convexity of W with respect to $\mathbf{C}$, so that the tangent matrix is always positive definite, the material parameters have to satisfy certain necessary conditions.

The quality of the fit between the experimental and theoretical data is measured with Eq. (19), the coefficient of determination R^2. This quality is the best when R^2 is closest to 1. This coefficient is built from residual sum S_{res} and the total sum S_{tot} of the least-squares by the number of points in experimental data n :

$$R^2 = 1 - \frac{S_{res}}{S_{tot}}. \tag{19}$$

$$S_{res} = \sum_{i=1}^{n}(\sigma_i^{exp} - \sigma_i^{an}(a_3, a_4, a_5, a_6, a_7, a_8, a_9))^2. \tag{20}$$

$$S_{tot} = \sum_{i=1}^{n}(\sigma_i^{exp} - \overline{\sigma}_i^{exp})^2. \tag{21}$$

σ^{an} is the vector from Eq. (17) and Eq. (18), σ^{exp} is the experimental data vector from superficial femoral artery biaxial tensile test [14] and $\overline{\sigma}^{exp}$ is the mean of experimental data:

$$\overline{\sigma}^{exp} = \frac{1}{n}\sum_{i=1}^{n}\sigma_i^{exp}. \tag{22}$$

Table 1 contains the parameters obtained in 30.64 seconds after 116 optimization iterations with $R^2 = 0.99$.

Table 1: Polyconvex deformation energy density function: material parameters

	a_3	a_4	a_5	a_6	a_7	a_8	a_9
Material parameters (kPa)	-2015.83	241.2	131.56	286.9	-87.1	75.69	-34.73

6 Validation of the model with two simulation examples

6.1 Biaxial tensile test

Only one eighth of the soft tissue sample is discretised. Symmetry conditions are applied and stretches (λ_{11}=λ_{22}= 1.1) are imposed respectively (Figure 3) along the $\vec{e_1}$ and $\vec{e_2}$ axes. The mesh uses 8-node hexahedral elements. Figure 3 represent the stress according to stretches on the FER/View post-processor [16].

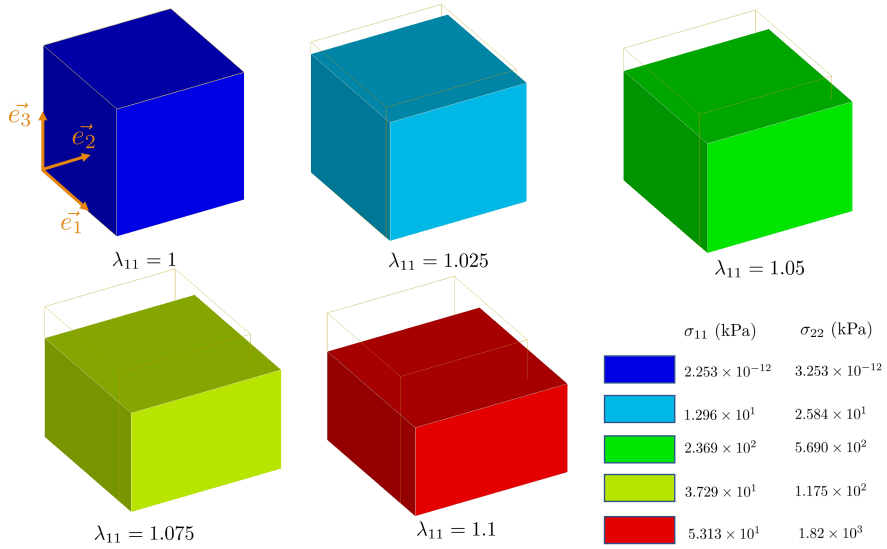

Figure 3: Biaxial simulation results depending on stretch λ_{11}

The numerical results obtained with FER are compared with the semi-analytical and experimental results. Figure 4 shows the stresses σ_{11} and σ_{22} as a function of the stretches λ_{11} and λ_{22}. This figure

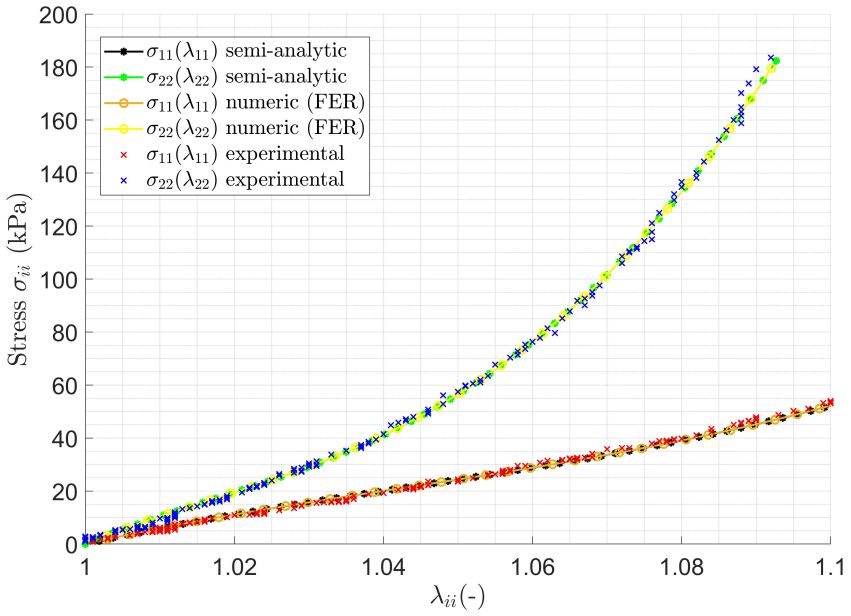

Figure 4: Comparison of stresses (Semi-analytic, numeric, experimental) σ_{11} and σ_{11} as a function of the stretches λ_{11} and λ_{22}

shows that with the identified parameters of table 1, experimental data, semi-analytic stresses Eq. (17) and Eq. (18), numerical results obtained with FER are in perfect agreement. No convergence problem has been encountered with the polyconvex law. The anisotropy of the model appears clearly. The corresponding stresses are different for the same stretch in the two directions.

The parameters used (Table 1) are very different from those found by Cai et al. [9, 10]. Figure 5 represent the comparison between two results using two sets of parameters. $\sigma_{ii}\,\mathrm{FER}_1$ represent the tensile simulation result from the set got from table 1. $\sigma_{ii}\,\mathrm{FER}_2$ are result using Cai et al.[10] parameters on the simulation. The results are closer to the experimental data compared to the original ones in [9].

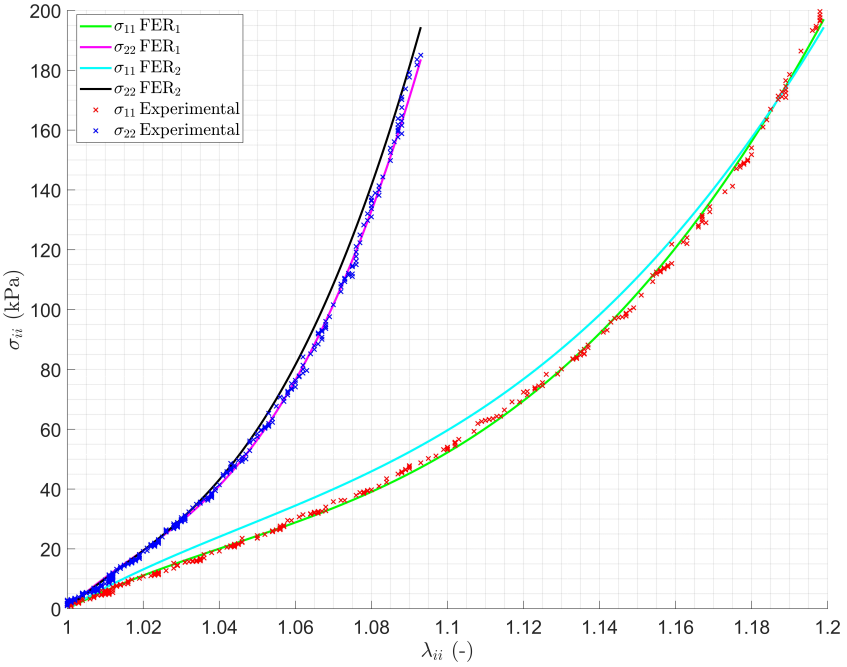

Figure 5: Comparison of simulation results using two different sets of parameter material

6.2 Indentation test

This test is simulated using the bipotential contact law [11], a law that couples contact and friction while eliminating interpenetration between bodies. This law was proved to be very efficient in contact treatment. Above all, it is not an intrusive method. The tangent matrices, according to (14), are not modified.

The test represents a rigid half-sphere applied to the artery. The radius of the sphere is 2.5 µm. The deformable-body is a paralleled-rectangles (Figure 2) of dimensions 10 µm × 4 µm× 10 µm. The mesh has 3 024 nodes and comprises 2 112 hexahedral elements of 8 nodes. The coefficient of friction between the soft tissue and the indenter is fixed at $\mu = 0.34$.

One hundred increments apply the load with a displacement of 0.01 µm at each step. Thus, the indenter undergoes a total vertical displacement of 1 µm. Qualitative results are presented in Figure 6, the directions of the four fibres are visible: the displacement distribution according to $\vec{e_3}$.

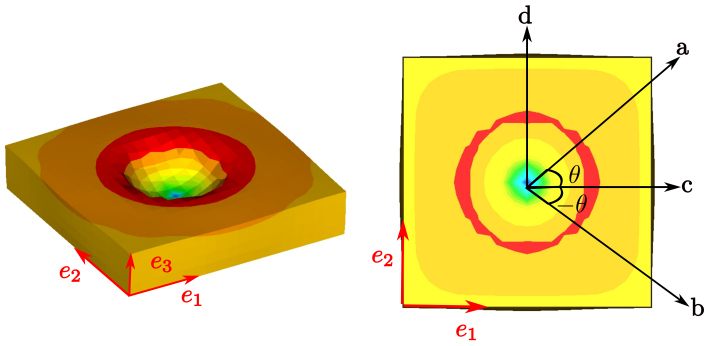

Figure 6: Direction of the 4 fibres families / Displacement according to $\vec{e_3}$ during the indentation test

7 Comparison of the polyconvex law with other hyperelastic laws

Figure 7 represents a biaxial simulation using the two hyperelastic anisotropic models: HGO-Yeoh and Polyconvex. For both models, the fitting with experimental data is suitable. Therefore, these laws are relevant to the modelling of anisotropic soft tissue.

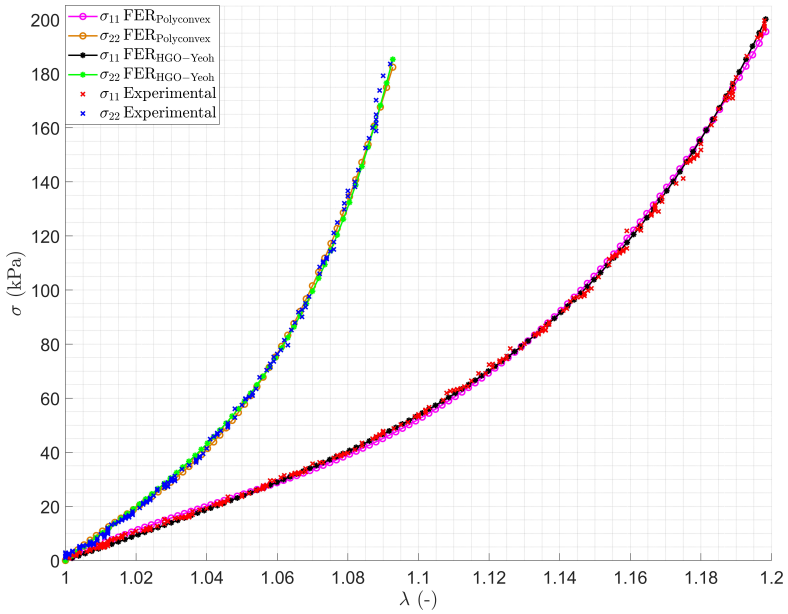

Figure 7: Comparison of the law HGO-Yeoh and Polyconvex results accuracy

Three behaviour laws, Polyconvex [9], Yeoh [6], and HGO-Yeoh [17] are compared from the CPU time point of view. The two examples (uniaxial tensile test and indentation test) described above (Section 6) were performed with the same F. E. code and computer. For each law, the times shown in Table 2 are the average of ten simulations.

Regarding the identification time in table 2, the parameters of the polyconvex law are obtained the fastest. The polyconvex law performs very well with times comparable with the Yeoh law, which is simpler and only isotropic for the simulation tests. The HGO-Yeoh law has an exponential form which makes the calculation slower. The polyconvex law is formulated by a polynomial form and uses polyconvex invariants that allow a fast convergence. Improvements are still possible, some calculations can be done outside the Newton-Raphson loops.

Table 2: Performances (CPU time) comparison of hyperelastic laws

Hyperelastic law	Yeoh	HGO-Yeoh	Polyconvex
Anisotropy	Isotropic	Anisotropic	Anisotropic
Nb of fibre's familly	–	1	4
Nb of parameters	3	5	7
Identification time	27.61 s	40.03 s	25.68 s
Tensile simulation time	3.33 s	7.68 s	4.85 s
Indentation simulation time	9 min 56 s	10 min 39 s	8 min 48 s

8 Conclusions

The polyconvex deformation energy density function (6) is a simple polynomial expression that allows easy implementation. This formulation also guarantees the tangent stiffness matrix's invertibility and the solution's uniqueness at each iteration during the numerical solution. This modelling enables uniques material parameters valid for all mechanical tests (tensile and shear, for example), which is not the case with other behaviour laws. This model remains limited when the stretches are very large. This new polyconvex behaviour law is very promising because of its robustness and speed in numerical simulation, which has been observed in treating contact problems with friction. The extensions of this work are the evaluation of more complex problems (adhesion, dynamics...) based on experimental data of other soft tissues.

References

[1] J. Lin, Y. Shi, Y. Men, X. Wang, J. Ye, and C. Zhang. Mechanical roles in formation of oriented collagen fibers. *Tissue Engineering Part B: Reviews*, 26(2):116–128, 2020.

[2] F. Xu and T. Lu. *Introduction to Skin Biothermomechanics and Thermal Pain*. Springer, 2011.

[3] M. Mooney. A theory of large elastic deformation. *Journal of Applied Physics*, 11(9):582–592, 1940.

[4] R. S. Rivlin. Large elastic deformations of isotropic materials iv. further developments of the general theory. *Philosophical Transactions of the Royal Society of London. Series A, Mathematical and Physical Sciences*, 241(835):379–397, 1948.

[5] E. M. Arruda and M. C. Boyce. A three-dimensional constitutive model for the large stretch behavior of rubber elastic materials. *Journal of the Mechanics and Physics of Solids*, 41(2):389 – 412, 1993.

[6] O. Yeoh. Some forms of the strain energy function for rubber. *Rubber Chemistry and Technology*, 66:754–771, 1993.

[7] A. N. Gent. A New Constitutive Relation for Rubber. *Rubber Chemistry and Technology*, 69(1):59–61, 03 1996.

[8] G. A. Holzapfel, T. C. Gasser, and R. W. Ogden. *A new Constitutive Framework for Arterial Wall Mechanics and a Comparative Study of Material Models*, chapter 61, pages 1–48. Springer Netherlands, Dordrecht, 2001.

[9] R. Cai, F. Holweck, Z.-Q. Feng, and F. Peyraut. A simple polyconvex strain energy density with new invariants for modeling four-fiber family biomaterials. *International Journal of Solids and Structures*, 115-116:126–139, June 2017.

[10] R. Cai, F. Holweck, Z.-Q. Feng, and F. Peyraut. Convexity, polyconvexity and finite element implementation of a four-fiber anisotropic hyperelastic strain energy density – Application to the modeling of femoral, popliteal and tibial arteries. *Preprint*, 2021.

[11] G. De Saxcé and Z.-Q. Feng. The bipotential method: A constructive approach to design the complete contact law with friction and improved numerical algorithms. *Mathematical and Computer Modelling*, 28(4-8):225–245, August 1998.

[12] Z.-Q. Feng, B. Magnain, and J.-M. Cros. FER/Impact : Logiciel de simulation numérique des problèmes d'impact. *Revue Européenne de Mécanique Numérique/European Journal of Computational Mechanics*, 15(1-3):175–186, 2006.

[13] J.-C. Simo and T.J.R. Hughes. *Computational Inelasticity*. Springer-Verlag New York, 1998.

[14] A. V. Kamenskiy, I. I. Pipinos, Y. A. Dzenis, C. S. Lomneth, S. A. Kazmi, N. Y. Phillips, and J. N. MacTaggart. Passive biaxial mechanical properties and in vivo axial pre-stretch of the diseased human femoropopliteal and tibial arteries. *Acta Biomaterialia*, 10(3):1301–1313, March 2014.

[15] Matlab optimization toolbox, 2020b. The MathWorks, Natick, MA, USA.

[16] Z.-Q. Feng, B. Magnain, J.-M. Cros, and P. Joli. Energy dissipation by friction in dynamic multibody contact problems. *COMPUTATIONAL MECHANICS*, page 9, September 2004.

[17] W. Alliliche, C. Renaud, J.-M. Cros, and Z.-Q. Feng. An anisotropic hyperelastic model for human skin: finite element modelling, identification of parameters, mechanical tests. In *Abstract book of International Symposium the 17^{th} on computer methods in biomechanics and biomedical Engineering and the 5^{th} Conference on imaging and visualisation*, page 118, 2021.